The Oxford space environment goniometer: A new experimental setup for making directional emissivity measurements under a simulated space environment

T. J. Warren, N. E. Bowles, K. Donaldson Hanna, and I. R. Thomas

Citation: Review of Scientific Instruments **88**, 124502 (2017); doi: 10.1063/1.4986657
View online: https://doi.org/10.1063/1.4986657
View Table of Contents: http://aip.scitation.org/toc/rsi/88/12
Published by the American Institute of Physics

REVIEW OF SCIENTIFIC INSTRUMENTS **88**, 124502 (2017)

The Oxford space environment goniometer: A new experimental setup for making directional emissivity measurements under a simulated space environment

T. J. Warren,[1,a)] N. E. Bowles,[1,a)] K. Donaldson Hanna,[1,a)] and I. R. Thomas[2,b)]
[1]*Atmospheric, Oceanic and Planetary Physics Department, University of Oxford, Oxford, United Kingdom*
[2]*Belgian Institute for Space Aeronomy (BIRA-IASB), Brussels, Belgium*

(Received 6 June 2017; accepted 28 October 2017; published online 8 December 2017)

Measurements of the light scattering behaviour of the regoliths of airless bodies via remote sensing techniques in the Solar System, across wavelengths from the visible to the far infrared, are essential in understanding their surface properties. A key parameter is knowledge of the angular behaviour of scattered light, usually represented mathematically by a phase function. The phase function is believed to be dependent on many factors including the following: surface composition, surface roughness across all length scales, and the wavelength of radiation. Although there have been many phase function measurements of regolith analog materials across visible wavelengths, there have been no equivalent measurements made in the thermal infrared (TIR). This may have been due to a lack of TIR instruments as part of planetary remote sensing payloads. However, since the launch of Diviner to the Moon in 2009, OSIRIS-Rex to the asteroid Bennu in 2016, and the planned launch of BepiColombo to Mercury in 2018, there is now a large quantity of TIR remote sensing data that need to be interpreted. It is therefore important to extend laboratory phase function measurements to the TIR. This paper describes the design, build, calibration, and initial measurements from a new laboratory instrument that is able to make phase function measurements of analog planetary regoliths across wavelengths from the visible to the TIR. *Published by AIP Publishing.* https://doi.org/10.1063/1.4986657

I. INTRODUCTION

A. The Diviner lunar radiometer

The initial motivation for this work is to provide laboratory support measurements for remote sensing observations of the Moon by the Diviner Lunar Radiometer ("Diviner"). Diviner is a nine-channel mapping radiometer on board NASA's Lunar Reconnaissance Orbiter (LRO) that has been orbiting the Moon since 2009.[1] The Diviner channels range across the ultraviolet to the visible (0.35 μm) and to the far infrared (400 μm) with three narrow channels centred on the thermal infrared (near 8 μm).

One of Diviner's main goals was to explore the possibility of water ice and other volatiles present in permanently shaded craters (PSCs) at the poles of the Moon. It has been shown that PSCs exist at the lunar poles due to the low axial tilt of the Moon's orbit relative to the Sun. It is believed these PSCs have not been exposed to direct sunlight for billions of years and hence are sufficiently cold to retain water ice (<120 K) and other volatiles delivered to the surface by comets and meteorites.[2–6] The main heating source for PSCs is reflected visible and re-radiated TIR from surrounding sunlit surfaces. Modeling the surface temperature in PSCs therefore requires a good knowledge of how TIR is scattered from sunlit surfaces into PSCs.

Although this paper focuses on the importance of TIR scattering at the lunar poles, understanding TIR scattering from the lunar surface is also important outside the lunar polar-regions since the hemispherically integrated emissivity affects the energy balance at the surface across all latitudes. Knowledge of TIR scattering from the surface also helps us to better estimate the surface temperature from radiance measurements. This is especially important with the large amounts of off-nadir observations that are planned for the Hayabusa-2, BepiColombo, and OSIRIS-REx missions.[7–9] These missions all have thermal infrared spectrometers or radiometers on board, and to fully extract all available information from their measurements, they must be compared with measurements made in the laboratory by infrared goniometers such as the one described in this paper.

B. 3D thermophysical models

Comparing the Diviner bolometric[24] surface temperature measurements with the results of three-dimensional thermophysical models allows constraints to be placed on the bulk properties of the top few centimetres[25] of the lunar surface. Such properties include the following: surface temperature, rock abundance, surface roughness, emissivity, density, and composition.[2,6,10–12] Three-dimensional thermophysical models of the lunar surface, such as the model developed by Vasavada *et al.*,[2] represent craters as a grid of surface elements. The one-dimensional thermal diffusion equation is then solved for each element with the assumption that each element re-radiates isotropically. If the modeled surface is flat then the re-radiation has no effect, however, if the surface is curved, like a cratered surface, then the re-radiation causes other elements of the surface to warm up. The re-radiation effect

[a)]warren@atm.ox.ac.uk; bowles@atm.ox.ac.uk; and kerri.donaldsonhanna@physics.ox.ac.uk
[b)]ian.thomas@aeronomie.be

is of importance on the lunar surface at high latitudes (>70°), where there is very little direct sunlight incident on the surface and reflected sunlight and re-radiated TIR emission from the local topography is the main driver in the observed surface temperatures.

A state of the art three-dimensional thermophysical model that accounts for re-radiation effects from the lunar surface is compared with the Diviner surface temperature observations in the work of Paige *et al.*[6] Systematic discrepancies of up to 20 K between the model and the Diviner surface temperature measurements were found in regions (>70° latitude) on the lunar surface where scattering is important. Paige *et al.*[6] states that the most likely reason for the discrepancy between Diviner measured temperatures and modeled temperatures is due to the unrealistic scattering properties used in the model. Accurate three-dimensional thermophysical models of the lunar environment require a realistic treatment of both (1) reflected solar light from adjacent surfaces incident and absorbed on the area of interest and (2) emitted TIR radiance from adjacent surfaces incident and absorbed on the area of interest.

Therefore, we have developed an instrument known as the Oxford Space Environment Goniometer (OSEG) to measure how TIR energy is emitted and re-emitted from surfaces for the inclusion into three-dimensional thermophysical models.

C. Bidirectional reflectance distribution function and directional emissivity definition

Before describing the setup and results from the newly developed OSEG, this section defines the terminology used to describe how radiation is scattered from a surface at different wavelengths and observational angles.

The bidirectional reflectance distribution function (BRDF) describes how visible and near infrared (VNIR) light is scattered from a surface for all viewing angles (azimuth, reflection, and incidence, see Fig. 1). It is defined [Eq. (1)] as the ratio of the scattered radiance at the detector to the collimated incident irradiance illuminating the surface[13]

$$r\left(\theta_r, \theta_i, \theta_p\right) = \frac{E_r(\theta_r, \theta_p)}{L_i(\theta_i, \theta_p)}, \tag{1}$$

where $r\left(\theta_r, \theta_i, \theta_p\right)$ is the BRDF, θ_r, θ_i, and θ_p are the angles of reflection, incidence, and azimuth defined in Fig. 1. L_i is the irradiance incidence on the surface at incidence angle θ_i and E_r is the radiance reflected from the surface at reflection angle θ_r.

The directional emissivity (DE) describes how thermal and far infrared radiation is emitted, reflected, and re-radiated from a surface for all viewing angles (azimuth, emission, and incidence, see Figs. 2 and 3). Directional emissivity is also referred to as the emission phase function (EPF) in some previous studies.[14] There appears to be no consensus in the scientific literature on the terminology used to define the DE and a single uniform term for DE is difficult to define. Therefore for clarity, in this paper, the DE is split into two different categories:

1. Emission only directional emissivity (EDE),
2. Re-radiated directional emissivity (RDE)

The EDE describes how the emission of a hot surface (>0 K) heated from below varies with emission angle (Fig. 2). The EDE is defined in Eq. (2) as the ratio of the radiance emitted from the sample to the radiance that would be emitted by an ideal blackbody under the same laboratory conditions (e.g., surface temperature, wavelength range, and viewing angle). As the sample is heated from below, there is no incidence plane as there is no light source and the azimuth angle must be defined from an arbitrary plane (Fig. 2),

$$\varepsilon_d\left(\theta_e, \theta_p, T, \lambda\right) = \frac{E(\theta_e, \theta_p, T, \lambda)}{U_b(T, \lambda)}, \tag{2}$$

where ε_d is the directional emissivity function, E is the radiance emitted by the surface, U_b is the total radiance emitted by a blackbody at the same temperature as the surface, and θ_e, θ_p are the emission and azimuth angles defined in Fig. 2. T is the

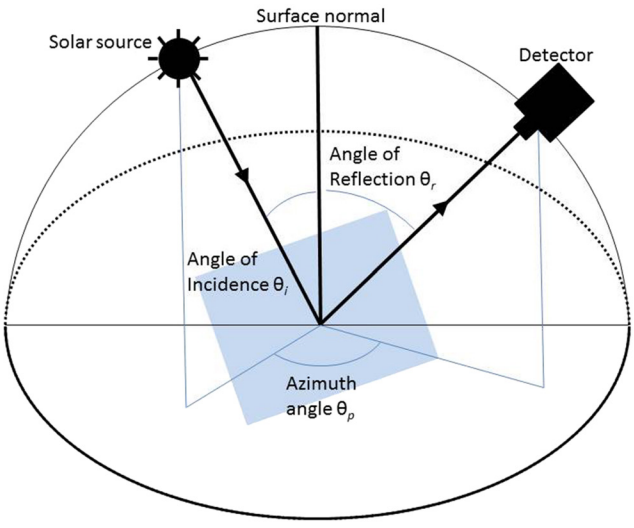

FIG. 1. Definition of all scattering angles for the bidirectional reflectance distribution function (BRDF).

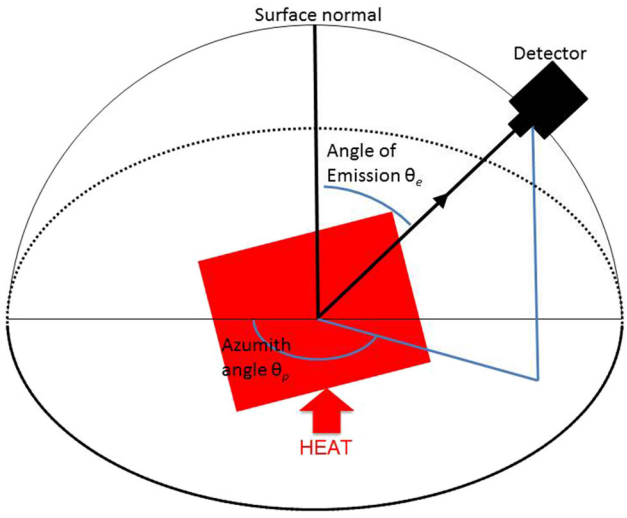

FIG. 2. Definition of scattering angles for directional emissivity when the surface is heated from below and is not illuminated. As there is no illumination source, the azimuth angle is defined from an arbitrary plane.

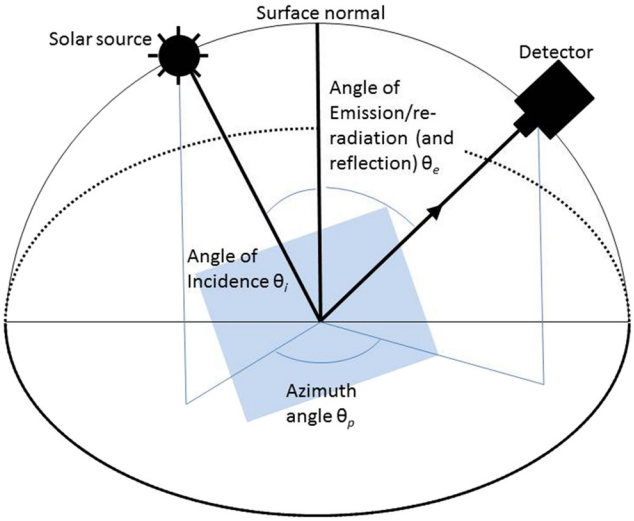

FIG. 3. Definition of all scattering angles for the RDE when the surface is heated from above by illumination.

temperature of the surface and λ is the wavelength range being measured.

Instead of being heated from below, a surface can also be heated by a radiation source from above. In this case, the radiation from a visible light source is absorbed and then re-radiated (or emitted) from the surface. The RDE describes how the surface re-radiates the absorbed light and is defined similarly to the EDE in Eq. (3) as the ratio of the radiance emitted by the sample to the radiance emitted by a blackbody under the same conditions (e.g., surface temperature, wavelength range, and viewing angle). It is important that the wavelength of the light source used does not overlap with the detector wavelength sensitivity. If the wavelength of the light source does overlap with the detector wavelength sensitivity, then some reflected radiation would be detected. The definition of RDE is strictly limited to how the surface re-emits radiation and does not include any contribution from reflected radiation,

$$\varepsilon_{dr}\left(\theta_e, \theta_p, \theta_i, T, \lambda\right) = \frac{E(\theta_e, \theta_p, \theta_i, T, \lambda)}{U_b(T, \lambda)}, \tag{3}$$

where ε_{dr} is the RDE, E is the radiance emitted by the surface, U_b is the total radiance emitted by a blackbody at the same temperature as the surface, and $\theta_e, \theta_p, \theta_i$ are the angles defined in Fig. 3. T is the temperature of the surface and λ is the wavelength range being viewed.

Although Eqs. (2) and (3) are adequate to describe the DE of a surface in the laboratory either heated from below or heated from a constant incidence angle, they are insufficient to describe the lunar surface. This is because they omit the illumination history of the surface. The Diviner nighttime measurements show that the lunar surface temperature is dependent on where and for how long the sun was in the sky on the previous day.[14] Even during the daytime surface temperatures, the previous illumination of the surface can still be important. This paper reports initial measurements from the OSEG of simple samples heated from below that therefore do not have an illumination history.

D. Previous goniometry work in the visible and near infrared with applications to planetary science

BRDF measurements of lunar regolith analogs and Apollo soils have been made before, in particular, by the Bloomsburg University goniometer (BUG)[15,16] and the PHIRE goniometer.[17] Measurements by both goniometers have shown that at VNIR wavelengths, the lunar regolith has anisotropic scattering at high incidence and emission angles (>45°).

Although PHIRE and BUG have made significant progress in measuring the BDRF of the lunar surface at VNIR wavelengths, laboratory measurements in the TIR and far infrared have yet to be done. The lack of data may be due to the lack of measurement data available from spatially resolved TIR instruments in orbit around airless bodies. Before Diviner, no spatially resolved remote sensing measurements of the lunar surface were available at multiple lunar times of day. The BUG and PHIRE goniometers are not designed to operate in the TIR so cannot be used to make DE measurements.

II. INSTRUMENTATION

A. Goniometer

The OSEG is designed to make automated measurements of a sample across wavelengths from the visible (500 nm) to the far infrared (400 μm), over as full a range of viewing angles (incidence, emission, and azimuth angles) as possible. The range of motion is determined by (Fig. 4) the following:

- *Azimuth angle movement*—A 360° ring mounted on a base plate, which rotates in both directions around the sample cup in the centre of the ring. The 360° ring is 650 mm in diameter.
- *Emission angle movement*—A 180° segment ring is placed vertically on top of the 360° ring. The radiometer is mounted onto a carriage, which is able to run up and down the 180° segment.
- *Incidence angle movement*—A 90° segment ring is place inside the 360° ring. The illumination source is mounted onto a carriage, which moves up and down the 90° segment.

Due to mechanical interference between the radiometer and base plate, the current goniometer design has limited motion in the incidence and emission angle direction. The currently available angular range of movement of the OSEG is given in Table I.

B. Radiometer and light source carriages

The OSEG is designed to work across wavelengths from the visible (500 nm) to the far infrared (400 μm) with interchangeable detectors and filters. This allows previous measurements done at visible wavelengths to be repeated to validate the setup as well as new measurements in the TIR to be made.

In this paper, two setups were used: one for measurements at visible wavelengths and the other for measurements in the TIR. For visible wavelengths, a green laser (Thorlabs stock number CPS532 – 532 nm) is setup nearby the goniometer on

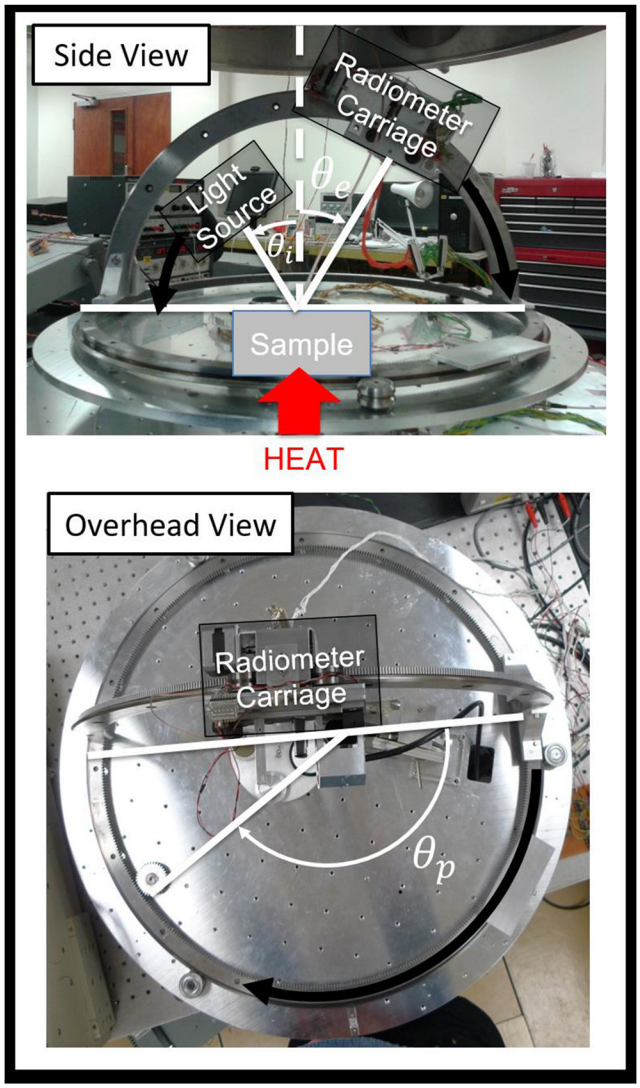

FIG. 4. OSEG setup on an optical bench showing the movement of the two arms allowing the angle of incidence θ_i, emission θ_e, and azimuth θ_p to be varied.

an optical bench. The laser light is then chopped and coupled down an optical fibre (Edmund optics #39-365). The optical fibre is then passed through a collimator (Edmund optics #53-042) on the light source carriage. This produces a small spot ~1 cm in diameter on the sample. The scattered radiation from the sample is then measured by the radiometer carriage (Fig. 5).

The radiometer carriage consists of a 90° off axis parabolic collecting mirror (Edmund optics #47-105) and a photodiode (RS stock number 0564021) placed at 33.8 mm behind the focal length of the collecting mirror to create a

TABLE I. The angular range of the OSEG.

	OSEG (deg)
Azimuth angle range	0–360
Emission angle range	0–75
Incident angle range	0–75

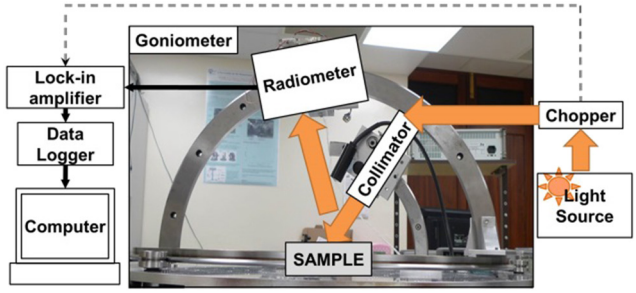

FIG. 5. Block diagram of the OSEG setup on an optical bench ready to make BRDF measurements at visible wavelengths of a Spectralon sample.

slightly converging (0.4°) input beam from the target onto the collecting mirror. The output of the photodiode is passed to a lock-in amplifier (Stanford Research Systems SR830) to deconvolve the output from the reference chopper signal. The output from the lock-in amplifier is then recorded on a PC.

This setup creates a field of view (FOV) on the sample at an emission/reflection angle of 0° that is much larger than the ~1 cm spot size of the light source. Therefore background radiation sources as well as the green laser light are observed inside the FOV of the radiometer carriage; however, these background sources do not affect the measurement as only radiation sources that are modulated at the chopping frequency (nominally 20 Hz) are recorded.

For measurements in the TIR, the light source carriage is removed and the sample is heated from below. The chopper is therefore moved to the radiometer carriage (Fig. 6). The photodiode is replaced with a pyro-electric (LIE-332f) TIR detector. A small baffle is placed on the radiometer carriage between the detector and collecting mirror to reduce the FOV such that at 0° emission angle it is 10 mm. As the radiometer carriage moves to increase the emission angle, the FOV will become ellipsoidal with a semi-major axis that increases with the cosine of the emission angle. Therefore at the maximum emission angle of the OSEG, 75°, the FOV will be 38.6 mm, this is smaller than the diameter of the samples used inside the OSEG (50 mm). For this TIR setup, the FOV has been accurately mapped out in the TIR using a pin hole hot source to show that the FOV is a well-defined circle with a diameter of 10 mm

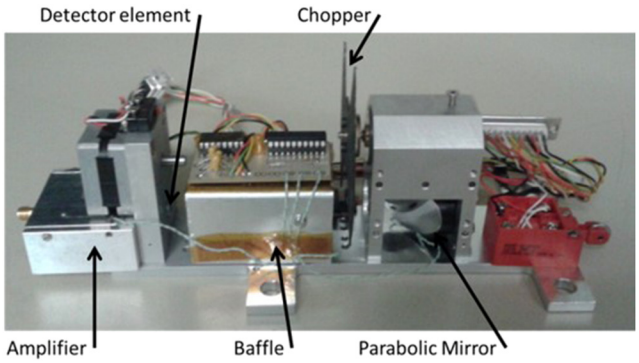

FIG. 6. Labeled diagram of the radiometer carriage setup for measurements in the TIR.

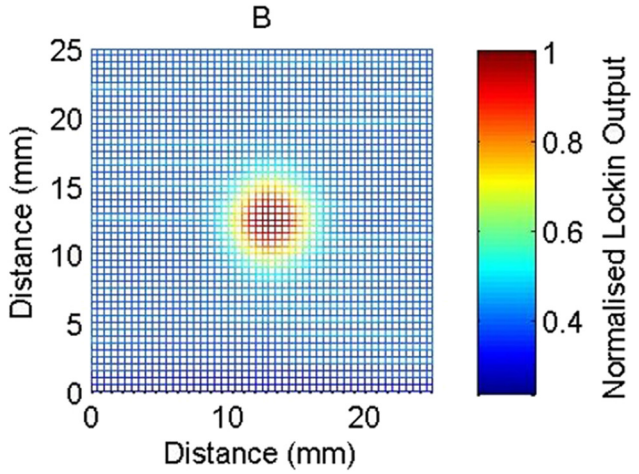

FIG. 7. Mapped FOV of the radiometer carriage at 0° emission angle. The FOV is a near perfect circle with a diameter of approximately 10 mm.

FIG. 8. Photographs showing thermal infrared setup. (Left) The OSEG setup inside the vacuum chamber without the cold shield surrounding it. (Right) The cold shield surrounded by 10 layers of multilayer insulation (MLI) house inside the vacuum chamber.

at an emission angle of 0° (Fig. 7). Wavelength selection in the TIR is currently provided by the KBr filter (0.2–25 μm) on the front of the detector element. For measurements in both the visible and TIR, the lock-in amplifier was set to a 1 s time constant and a settling time of 30 s was waited before recording the lock-in voltage.

For measurements in the TIR, the current setup of the OSEG does not include a light source. A light source is in development, but at the time of writing has not yet been implemented into the setup and therefore samples can only be heated from below. Because of the lack of a solar illumination source, the measurements made by the OSEG and described in this paper are only applicable to the night-time lunar surface and cannot be applied to the day-time surface. Once the light source is implemented in the OSEG, future measurements can then be applied to the daytime lunar surface temperature, which is dependent on the illumination angle.

C. Cold shroud and vacuum chamber

On the lunar surface, a strong thermal gradient (100 K) is induced in the top few hundreds of microns of the lunar surface (e.g., Refs. 12 and 18). This gradient is induced by the surrounding cold space and vacuum environment found on the lunar surface. This thermal gradient could have large implications for the emission and re-emission of TIR. We therefore developed the OSEG to fit inside a 1 m cold thermal shroud (<150 K) which can simulate the cold of space (Fig. 8). The cold shroud sits inside a vacuum (10^{-6} mbar) chamber that simulates the vacuum environment found around the Moon.

For measurements in the TIR, it is important that the sample is surrounded by a thermally stable shroud. For measurements made in the visible, background radiance can be removed by chopping the light source; however, in the thermal infrared, this is not possible as there is no light source. To measure the DE, all measurements at all different emission angles are normalised to the measurement at 0° emission angle (i.e., looking straight down at the sample). Therefore provided the background radiance across TIR wavelengths does not change between measurements at different angles, then the background radiance will be removed in the normalisation process.

When the cold shroud is on, it is important that the shroud is at an isothermal temperature to simulate the lunar environment. Thermal modeling using the multi-physics package COMSOL has shown that the temperature difference between the top and the bottom of the cold shroud is approximately 3 K and has been confirmed experimentally.

III. VALIDATION USING STANDARD TARGET AT VISIBLE WAVELENGTHS

Before DE measurements in the TIR were made using the OSEG, the setup was validated at visible wavelengths by making measurements of the well-characterised commercial reference target sample Spectralon (Labsphere, Inc.).

A. BRDF measurement of Spectralon with visible illumination (625 nm)

For visible wavelengths, the OSEG setup has been tested by measuring the BRDF of a calibrated Spectralon^{TM} target and comparing the reflectance measurements to the measurements made of a similar target by the PHIRE goniometer.[17] Over the currently accessible angular range of the OSEG, there is good agreement (within 1σ) between the two sets of measurements. The PHIRE goniometer has previously been validated using a similar technique to measurements made by the BUG goniometer.

The calibration of OSEG measurements has been carried out in an identical way to the PHIRE goniometer, which is summarised here. All measurements made by PHIRE are calibrated by assuming that the BRDF of Spectralon is equal to 0.99 (its hemispherical albedo) at an incidence angle of 0° and an emission angle of 55° over the entire visible and

near-infrared (0.4–2.5 μm) spectral range. All reflectance measurements made by PHIRE are then calibrated relative to this single reference measurement.

For visible wavelength measurements, the OSEG uses a modulated light source (20 Hz) that provides a small (1 cm) well-defined spot size on the sample. The diameter of the Spectralon sample is 5 cm. At an emission angle of 0°, the FOV of the radiometer is larger than the surface of the sample and when the emission angle increases, the FOV becomes ellipsoidal, with the length of the semi-major axis proportional to the cosine of the emission angle. Areas outside the sample are therefore in the FOV, but do not contribute to the signal, as they are not illuminated by the modulated light source. The general optical layout chosen for the OSEG is identical to the PHIRE instrument (small incident beam and large detector FOV) and implies a division by the cosine of the emission angle to retrieve the BRDF [Eq. (4)] or reflectance factor values [Eq. (6)] from the raw voltage V,

$$r(\theta_e, \theta_p, \theta_i) = C_\lambda V \frac{\cos(\theta_i)}{\cos(\theta_e)}, \tag{4}$$

where C_λ is a wavelength dependent calibration constant defined in Eq. (5), V is the raw voltage, θ_i and θ_e are the incidence and emission angles defined in Fig. 3,

$$C_\lambda = \frac{0.99\ \cos(55°)}{\pi V_{Sp,55°}}, \tag{5}$$

where $V_{Sp,55°}$ is the raw voltage at 55° emission angle and 0° incidence angle,

$$\bar{R} = \pi \frac{r(\theta_e, \theta_p, \theta_i)}{\cos(\theta_i)}, \tag{6}$$

where $\bar{R}$ is the reflectance factor and θ_i is the incidence angle Fig. 3.

The PHIRE measurements are calculated in both BRDF and reflectance factors values from the raw voltage measurements, according to the standard definitions used in Eqs. (4) and (6). According to these formulae, the BRDF of an ideal lambertian target would be equal to $\frac{1}{\pi \cos(\theta_i)}$ and the reflectance factor of the same target would be equal to 1, independent of both emission and incidence angles. The PHIRE goniometer measurements are normally reported in the reflectance factor, so this will therefore be used to compare the two measurements in this paper.

The reflectance factor of Spectralon was measured in steps of 5.7° emission, 12° azimuth, and 0° incidence angles. Unfortunately, due to the plastic container of the Spectralon, it was difficult to get the surface of the target aligned with the frame of the goniometer. However, it was possible to correct for this sample tilt using a method developed for the PHIRE goniometer.[17] A comparison between the measured reflectance factor of Spectralon (with the surface tilt removed) by PHIRE and the OSEG is displayed in Fig. 9. Measurements made by the OSEG agree within error to measurements made by PHIRE (R^2 of 0.95). The similarities between these two measurements validate the OSEG setup and shows it can make BRDF measurements with a comparable accuracy to PHIRE. The slight differences in the two measured values could be explained by small differences in the Spectralon targets used or be due to the different wavelengths used (the OSEG measurement was made at 523 nm and PHIRE was made at 650 nm).

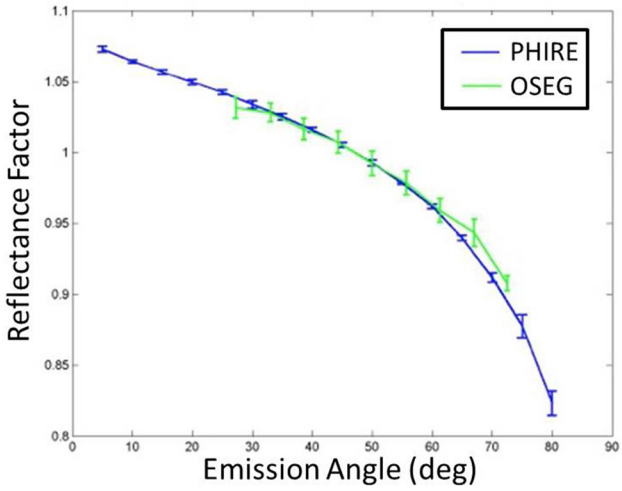

FIG. 9. Comparison between measured reflectance factor values of Spectralon by OSEG and PHIRE. The sample tilt has been removed from both sets of measurements using the method described in Ref. 17. The error bars represent the standard deviation of all the measured reflectance factor values at a particular emission angle, but at different azimuth angles.

IV. PRELIMINARY RESULTS OF SIMPLE NEXTEL BLACK PAINTED SURFACES

After completing the design, testing and validation of the OSEG, the DE measurements of a spray painted Nextel (Nextel paint manufactured by Mankiewicz Gebr. & Co.) aluminium target was made. The Nextel painted surfaces were chosen as the first DE measurement of a surface made by the OSEG because its DE has previously been characterised.[19–21]

The Nextel target was constructed by covering the surface of a 50 mm diameter, 5 mm thick aluminium plate with four layers of Nextel–Velvet-Coating 811-21. CSY Finishes

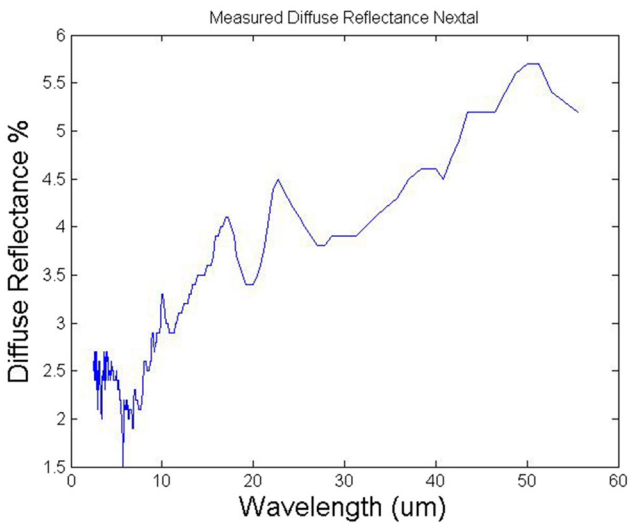

FIG. 10. The diffuse reflectance of Nextel 81-211 velvet black paint as measured by the National Physics Laboratory (NPL). Emissivity of Nextel was calculated as one minus the reflectance. After Ref. 22.

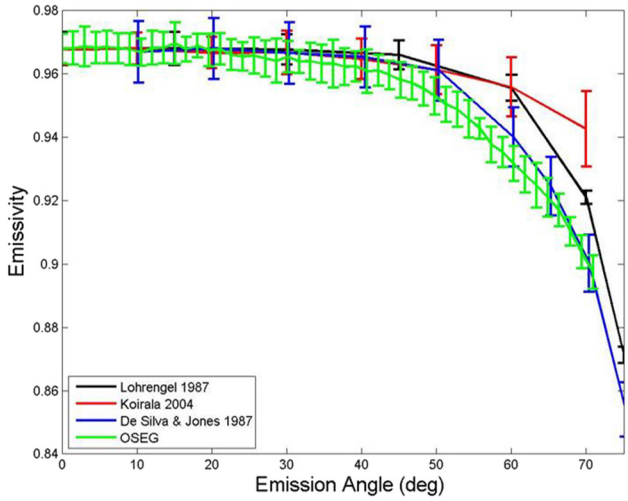

FIG. 11. Comparison between DE measurements of Nextel black paint by OSEG and other IR goniometers.[20,21,23]

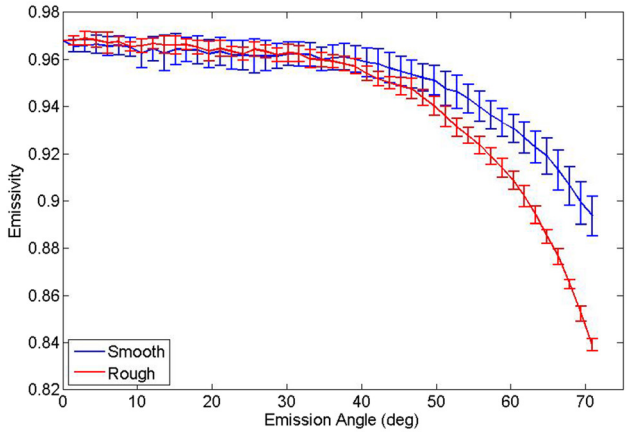

FIG. 13. DE measurements of two Nextel targets with different surface roughness profiles. The error bars are calculated from the standard deviation of all measurements made at that emission angle. For each run, ten measurements are made at each emission angle as the radiometer carriage moves down and ten measurements are made at each emission angle as the radiometer moves up.

(a professional spray painting company) applied the paint using a spray pistol to produce an almost uniform thickness over the surface.

According to the definition of directional emissivity (DE) [Eq. (2)], the radiation emitted by the sample is compared with that emitted by an ideal blackbody, under the same conditions. However, with the OSEG setup, it is sufficient to compare the emitted radiation at each emission angle to the radiation emitted from the Nextel disk at 0° emission angle. At an emission angle of 0°, the emissivity of Nextel is assumed to be equal to 0.968. This value is calculated by convolving the Planck function at the measured temperature of the target, the spectral response of the KBr (0.2–25 μm) window, and the normal emissivity of Nextel (Fig. 10). Using 0.968 as the normal emissivity of Nextel (emission angle of zero), the DE can then be calculated as

$$\varepsilon_d(\theta_e, T) = 0.968 \frac{V(0°, T)}{V(\theta_e, T)}, \tag{7}$$

where $\varepsilon_d(\theta_e, T)$ is the DE, $V(\theta_e, T)$ is the recorded raw lock-in voltage, and V(0°, T) is the raw lock-in voltage recorded at 0° emission angle. By this equation, an isotropic surface emitter will have a DE of 0.968 for all emission angles.

The DE of the Nextel-Velvet-Coating 811-21 was measured using the OSEG system (Fig. 11).[26] It is clear from the goniometer measurements by OSEG that Nextel is not an isotropic emitter. At emission angles greater than 40°, the emissivity of Nextel diverges significantly (Δ0.01 at 40° and Δ0.08 at 70°) from the expected emissivity of an isotropic emitter. As stated before, three previous measurements of the DE of Nextel painted targets have been made with three different goniometer systems similar to the OSEG setup.[19–21] The three measurements are compared to the OSEG measurement in Fig. 11. All four measurements agree within error between 0° and 50° emission angles. However at emission angles greater than 50°, there is some variation between the measurements and at 70° there is a difference in an emissivity of 0.04 between the measurements. The measurement made by De Silva and Jones[21] agrees best with the OSEG measurement ($R^2 > 0.99$) and is in agreement (within error) with the OSEG measurement over the entire measured angular range. The variation between measurements at high emission angles with the other two measurements could be due to slight differences in the surface texture of the Nextel paint used.

Further evidence for this is provided from the measurement of a roughly painted Nextel sample. A second "rough" Nextel target was made by roughly painting a 50 mm diameter aluminium base. This created a different texture to the CSY spray painted "smooth" target. Compared to the "smooth" target, the "rough" target contained roughness features on the

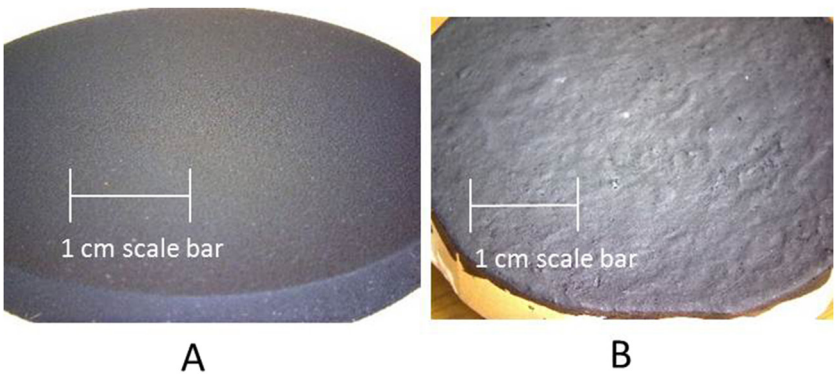

FIG. 12. (a) Smoothly spray painted and (b) roughly painted Nextel Velvet black aluminium target 50 mm in diameter.

1-10 mm scale (Fig. 12). The DE of the rough target is significantly different compared to the smooth target, suggesting that surface roughness is an important parameter in the DE of a surface (Fig. 13).

V. CONCLUSIONS

Visible BRDF measurements of the Spectralon reflectance standard have been made using a new goniometer setup, OSEG, and compared with similar measurements made by the PHIRE goniometer. The measurements agree within error, validating the OSEG setup at visible wavelengths.

New broad TIR measurements of the DE of Nextel paint have been made using the OSEG. Three previous measurements show a large spread in the DE for emission angles greater than 45°. Our results suggest that the reason for this spread is due to differences in the surface roughness of the measured Nextel samples. The anisotropic scattering observed in the measurements of the black Nextel targets suggests that the lunar regolith is unlikely to scatter isotropically. Bandfield *et al.*[14] has previously reported anisotropic scattering from the lunar surface in the Diviner data set. The brightness temperature measured by Diviner decreases with increasing emission angle from all azimuth angles in both the day and night time data. The measurements made in this paper provide clear supporting evidence for this anisotropic scattering effect.

Anisotropic scattering from the lunar surface will have large implications for the three-dimensional thermophysical models that try to reproduce the surface and subsurface temperature of the lunar soil. However, further modeling work is required to fully understand the impact of this on the modeled lunar surface temperature. Quantitatively one would expect this result to reduce the amount re-radiated TIR emitted from illuminated topographical features into un-illuminated regions. Hence the surface temperatures in un-illuminated regions should decrease.

This work has also shown that surface roughness is an important factor in the DE of a surface. However, further work is required to investigate this further. Particularly, which length scales are important, sub-millimetre or larger centimetres.

Finally, the large amount of off-nadir data expected from the TIR instruments on board the Hayabusa-2, BepiColombo, and OSIRIS-Rex missions will require comparisons to laboratory measurements. The newly developed TIR goniometer system described in this paper will be able to provide those measurements.

ACKNOWLEDGMENTS

The authors would like to thank the UK Science and Technology Facilities Council and the Leverhulme Trust research grant RPG-2012-814 for their support in preparing this study.

[1]D. Paige *et al.*, "The lunar reconnaissance orbiter Diviner lunar radiometer experiment," Space Sci. Rev. **150**, 125–160 (2009).
[2]A. R. Vasavada, D. A. Paige, and S. E. Wood, "Near-surface temperatures on Mercury and the Moon and the stability of polar ice deposits," Icarus **141**, 179–193 (1999).
[3]J. Arnold, "Ice in the lunar polar regions," J. Geophys. Res. **84**, 5659, doi:10.1029/jb084ib10p05659 (1979).
[4]K. Watson, B. Murray, and H. Brown, "The behavior of volatiles on the lunar surface," J. Geophys. Res. **66**, 3033, doi:10.1029/jz066i009p03033 (1961).
[5]M. A. Siegler, B. G. Bills, and D. A. Paige, "Effects of orbital evolution on lunar ice stability," J. Geophys. Res. **116**, E03010, doi:10.1029/2010je003652 (2011).
[6]D. Paige *et al.*, "Diviner lunar radiometer observations of cold traps in the Moon's south polar region," Science **330**, 479–482 (2010).
[7]D. Lauretta and O. Team, "An overview of the OSIRIS-REx asteroid sample return mission," Lunar Planet. Inst. Sci. Abstract 2491, 5–6 (2012).
[8]H. Hiesinger and J. Helbert, "The Mercury radiometer and thermal infrared spectrometer (MERTIS) for the BepiColombo mission," Planet. Space Sci. **58**, 144–165 (2010).
[9]Y. Tsuda, M. Yoshikawa, M. Abe, H. Minamino, and S. Nakazawa, "System design of the Hayabusa 2—Asteroid sample return mission to 1999 JU3," Acta Astronaut. **91**, 356–362 (2013).
[10]J. L. Bandfield *et al.*, "Lunar surface rock abundance and regolith fines temperatures derived from LRO Diviner Radiometer data," J. Geophys. Res. **116**, E00H02, doi:10.1029/2011je003866 (2011).
[11]T. D. Glotch *et al.*, "The Mairan domes: Silicic volcanic constructs on the Moon," Geophys. Res. Lett. **38**, L21204, doi:10.1029/2011gl049548 (2011).
[12]I. R. Thomas *et al.*, "A new experimental setup for making thermal emission measurements in a simulated lunar environment," Rev. Sci. Instrum. **83**, 124502 (2012).
[13]B. Hapke, *Theory of Reflectance and Emittance Spectroscopy* (Cambridge University Press, 2014).
[14]J. L. Bandfield, P. O. Hayne, J. Williams, B. T. Greenhagen, and A. David, "Lunar surface roughness derived from LRO Diviner radiometer observations," Icarus **248**, 357–372 (2015).
[15]M. Shepard, *Initial Results From the Bloomsburg University Goniometer Laboratory* (Astrophysics and Space Science Library, 2002), p. 17815.
[16]J. Johnson and M. Shepard, "Spectrogoniometric measurements and modeling of Apollo 11 soil 10084," Lunar Planet. Sci. Abstract 1427, 4–5 (2009).
[17]A. Pommerol *et al.*, "Photometry and bulk physical properties of Solar System surfaces icy analogs: The planetary ice laboratory at university of Bern," Planet. Space Sci. **59**, 1601–1612 (2011).
[18]B. G. Henderson and B. M. Jakosky, "Near-surface thermal gradients and their effects on mid-infrared emission spectra of planetary surfaces," J. Geophys. Res. **99**, 19063, doi:10.1029/94je01861 (1994).
[19]J. Lohrengel, *Gesamtemissionsgrad von Schwiirzen* (Springer-Varlag, 1987), Vol. 21, pp. 311–315.
[20]L. R. Koirala, *Ftir-Spectroscopic Measurement of Directional Spectral Emissivities of Microstructured Surfaces* (University of the Federal Armed Forces Hamburg, 2004).
[21]A. De Silva and B. Jones, "The directional-total emittance at 368 K of some metals, solar absorbers and dielectrics," J. Phys. D: Appl. Phys. **20**, 1102–1108 (1987).
[22]F. Clarke, "Certificate of calibration hemispherical, diffuse and regular spectral reflectances of one sample," National Physics Laboratory Report CETM/27/97, 1997.
[23]J. Lohrengel, "Total emissivity of black coatings," Heat Mass Transfer **315**, 311–315 (1987); [J. Lohrengel, "Gesamtemissionsgrad von Schwärzen," Wärme- und Stoffübertragung **21** , 311–315 (1987) (Original German publication)].
[24]The bolometric brightness temperature measured by Diviner is a measure of the spectrally integrated flux of infrared radiation emerging from the lunar surface and is different to the lunar surface temperature. Due to the poor thermal conductivity of the lunar surface, parts of the lunar surface that are in shadow can be at a significantly lower temperature (<150 K) than parts that are in direct sunlight (400 K). This large temperature gradient can exist across two parts of the surface that are only a few centimetres apart. Since the Diviner field of view is >400 m^2, the lunar surface will contain a wide variety of surface temperatures inside the field of view. The bolometric brightness temperature that Diviner measures is therefore a radiometric averaged temperature of a surface that is made up of elements at different temperatures.
[25]Typically the sensitivity is in the top few centimetres however it can extend to can extend to 10's of centimetre depths depending on the specific application.
[26]The measurement was made with the Nextel target at a temperature of 100 °C. The uniformity of the Nextel target was measured using a FLIR I50 thermal infrared camera and found to be uniform ±0.25 °C.